Composite Structures 185 (2018) 132–147

Contents lists available at ScienceDirect

Composite Structures

journal homepage: www.elsevier.com/locate/compstruct

Multi-objective multi-laminate design and optimization of a Carbon Fibre Composite wing torsion box using evolutionary algorithm

Sachin Shrivastava[a], P.M. Mohite[a,*], Tarun Yadav[b], Appasaheb Malagaudanavar[b]

[a] Department of Aerospace Engineering, Indian Institute of Technology Kanpur, UP 208016, India
[b] AURDC, Hindustan Aeronautics Limited, Nasik, MH 422207, India

ARTICLE INFO

Keywords:
Genetic algorithms
Wing torsion box
Multi-objective optimization
Carbon Fibre Composites
Smart tailoring
Python-scripting

ABSTRACT

The present study aims to minimize the weight of multi-laminate aerospace structures by a classical Genetic Algorithm (GA) interfaced with a CAE solver. The structural weight minimization is a multi-objective optimization problem subjected to fulfilling of strength and stiffness design requirements as well. The desired fitness function connects the multi-objective design requirements to form a single-objective function by using carefully chosen scaling factors and a weight vector to get a near optimal solution. The scaling factors normalize and the weight vector prioritizes the objective functions. The weight vector selection was based on a posteriori articulation, after obtaining a series of Pareto fronts by 3D hull plot of strength, stiffness and assembly weight data points. During the optimization, the algorithm does an intelligent laminate selection based on static strength and alters the ply orientations and thickness of laminae for faster convergence. The study further brings out the influence of mutation percentage on convergence. The optimization procedure on a transport aircraft wing torsion box has showed 29% weight reduction compared to an initial quasi-isotropic laminated structure and 54% with respect to the metallic structure.

1. Introduction

The aerospace structures like wing, fuselage, control surfaces, etc. are multi-laminated complex structural assemblies. The weight optimization of such structures is quite complex task as the design of such structures has to qualify for multiple design criteria. Thus, it is a multi-objective design optimization problem. Moreover, the estimation of design-values of different criteria for such structural problems by closed form solutions is not available. Therefore, the designer has to obtain approximate solutions. The finite element (FE) approximations using softwares like ABAQUS, NASTRAN, etc. are very popular due to their ease and therefore, widely used by designers. To reach optimal solution in multi-objective optimization problem (MOOP), multiple solutions by CAE solver are required in an unguided search environment, which may be highly time taking and inefficient. On the contrast, multi-objective optimization of mathematical problems using GA is well established. Now-a-days along with high speed computational facilities and structured FE meshes, numerical solutions have brought down computational time drastically. Therefore, in a step forward, if the power of evolutionary algorithms is coupled with CAE softwares, then smart tailoring of laminated aerospace structural assemblies can be accomplished. The resulting structural assemblies will be highly optimized lightweight in compliance with structural design requirements. However, as these design requirements are multi-objective in nature, it is difficult to establish trade-off to have an optimal solution. Moreover, in multi-laminated structures the strength and stiffness of assembled/co-cured structure are interdependent, hence, it is required to address such problems on a global basis. The Carbon Fibre Composites (CFC) lamina is highly anisotropic in strength and stiffness, which, in general, is used to form such tailored laminated structures.

In the present work, GA based optimization algorithm has been developed to optimize multi-objective multi-laminate wing structure, which can be applied to design other primary and secondary aircraft structures as well. The GA optimization idea has been well utilized by the authors for small single objective optimization problem of a control surface, where a laminated control surface was optimized for first ply failure index (FI) and achieved a weight benefit [1]. However, the real life problems are multi-objective in nature and one such problem for optimal design of wing structure for achieving minimum weight is addressed here. Deb [2] suggested mathematical expression for handling of MOOP, where a suitable single-objective function Z can be defined as a combination of several single objective functions f_i along with respective relative importance factors (weight factors) w_i as,

$$Maximize/Minimize\ Z = w_1 f_1 + w_2 f_2 + w_3 f_3 + ...+ w_i f_i \quad (1)$$

* Corresponding author.
E-mail address: mohite@iitk.ac.in (P.M. Mohite).

https://doi.org/10.1016/j.compstruct.2017.10.041
Received 30 May 2017; Received in revised form 3 September 2017; Accepted 12 October 2017

The solution to MOOP is obtained as Pareto optimal front of non-dominated solutions. However, deviating from Pareto front is trading off [3], where the decision maker imposes the preferences and classifies the objectivity of the problem which is governed by the choice of w_i.

The majority of researchers working on GA based design and optimization of laminate stacking sequence have attempted single objective laminate optimization, under different kind of loads and failure criteria [4–7]. However, researchers [8–10] have attempted multi-objective optimization of hybrid laminated plate structures along with FE solution to evaluate the fitness function. In aerospace domain, weight optimization along with deflection and fundamental frequency of laminated plate structures has been discussed in [11,12], respectively. Kim et al. [13] attempted multi-objective and multi-disciplinary design optimization of a supersonic fighter wing. Their study was based only on limited sets of design variables under aerodynamic and structural requirements. On similar lines, direct multi-search technique was used in [14] to get Pareto optimal of non-dominated set which is free of derivatives similar to GA. Gillet et al. [15] studied single and MOOP of composite structures for glass/epoxy UD and glass/epoxy fabric composite along with fibre orientations for a laminated plate under different loads and boundary conditions. They emphasised on ply orientation to be an important parameter during optimization. Hybrid laminated plate optimization was attempted by Kalantri [9] using NSGA II [16].

Blasques et al. [17] discussed MOOP for beams with rectangular, elliptical and box cross-sections. They did weight optimization along with eigenvalue of the structure by change in fibre angle in beam section [17]. This technique brought in nearly 800 fibre orientations as design variables for a beam problem with a 10 layered laminate. The implementation of this technique to multi-laminate optimization will result in a huge problem, which is practically impossible to handle. Although, there are many attempts in GA optimization using FE tools, but studies are primarily limited to plate and shell structures only. The GA based multi-objective optimization has been attempted in other engineering fields also by [18,19] for laminated structures. Apart from GA, ant-colony optimization [20] and artificial neural network [21,22] techniques are also available for optimizing single objective laminated plate structures.

In the present work, authors have attempted application of GA optimization for large aerospace structures like wing and fuselage, which is less explored for multi-objective optimization on assembly basis. This is done by demonstrating it over a transport aircraft wing torsion box (WTB) design. The implementation of multi-objective multi-laminate optimization for large complex structural assemblies like aircraft wing/fuselage has a lot of scope for weight reduction for future aircraft structures. The present industrial practice for design of stacking sequence uses pseudo-optimization, in which specific sets/combination of ply orientation are used to design the structure. The pseudo-optimal design sets are based on past aircraft design experiences, rather than domain search for optimal solution.

The formation of strings for GA based optimization using industrially preferred choice of fibre angles and solving it for failure criterion viz. Tsai-Wu first ply failure index (FI) (strength criterion) and wing tip deflection (stiffness criterion) D, is attempted in the present work. Such multi-objective multi-laminate problems have large number of design variables which are brought to a common platform. To start with optimization procedure, the initial metallic model was converted to an equivalent quasi-isotropic laminated structure after performing equivalent stiffness calculations having equal oriented fibres at 45°. The quasi-isotropic laminated FE model was a starting model, which is submitted to GA optimizer. The GA optimizer strings were defined to contain information about ply orientation and existence of a ply in terms of thickness. To delete a ply from the laminate, the thickness variable is assigned a dummy (near zero) thickness value during optimization after evaluation of laminate by analytical experiments. The orientation and thickness of laminates of initial sized model were

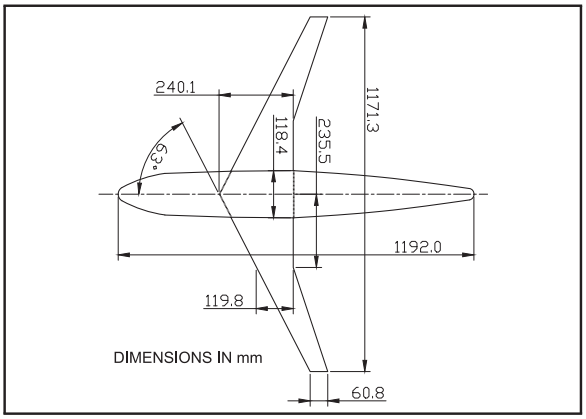

Fig. 1. DLR F6 wing/body planform.

defined in ABAQUS/CAE v6.11 Laminate-Modeler (LM). The LM was externally governed by MATLAB R2014a by a python-script and updated laminates are submitted for FE analysis for the estimation of design parameters to evaluate fitness function of the optimizer. The fitness function defined for GA optimizer was a weighted combination of structural weight, Tsai-Wu FI and wing tip deflection D after normalization.

Apart from the scaling, weight vector w_i was a part of objective function to prioritize the importance of the constraints during optimization. The weights w_i were essentially the fractional numbers such that $\sum_{i=1}^{N} w_i = 1$, where N is the number of objective functions in the final multi-objective function. During optimization the laminate with maximum FI (MFI) is identified at the end of each sub-loop, which guides the solution to optimize the identified laminate in its next iteration.

In the following sections, the basis for metallic wing torsion box design and its subsequent conversion into a quasi-isotropic laminated composite structure followed by the above mentioned optimization have been presented in details.

2. Design of WTB

The DLR-F6 geometry [23] given in Fig. 1 was selected to demonstrate the present optimization procedure. The selected geometry was a scaled version of typical transport aircraft DC-9. The DLR-F6 geometry details are available from AIAA Drag Prediction Workshop (DPW-III) [23,24]. The lift distribution acting on wing geometry was estimated through CFD simulations in ANSYS FLUENT 14.5 after a grid convergence study using ICEM-CFD software [25]. The pressure distributions obtained from the CFD simulations are applied as chordwise segmental pressure load over the wing geometry. The performance parameters of DC-9 aircraft by Endres and Douglous [26] are given in Table 1. The maximum take-off weight of 54.9 tons (including a design factor) was considered as a design load for the present study. The initial sizing [27] for WTB was done considering high strength aluminium alloy of aircraft grade having breaking stress $(\sigma_b) = 410\,MPa$, (yield stress)$\sigma_s = 294\,MPa$, and $E = 69\,GPa$ for maximum take-off weight of the vehicle and maximum D restricted to 10% of wing span [28] at design load. The details of initial sizing can be seen in [27].

Table 1
Basic data of DC-9 aircraft [26].

Length	40.72 m
Span	28.47 m
Wing semi-span	9.7 m
Width of Torsion Box	1.4 m
Height	8.53 m
Wing Area	92.97 m^2
Max take-off weight	54,900 kg

3. Conversion of WTB from metallic to a composite structure

A laminate is called quasi-isotropic when its extensional stiffness matrix behaves like an isotropic material. In case of classical laminates, this requires that $A_{11} = A_{22}$, $A_{16} = A_{26} = 0$ and $A_{66} = \frac{A_{11} - A_{12}}{2}$. Further, this extensional stiffness matrix is dependent on orientation of layers in the laminate. Laminates with $N(\geqslant 3)$ equal thickness layers and N equal angles between adjacent fibre orientations form the quasi-isotropic laminates. The N equal angles $\triangle\theta$ between the fibre orientations can be given as $\triangle\theta = \frac{\pi}{N}$ [29]. The reduced compliance matrix $[S]$ for the lamina in principal material directions using mechanical properties is given by

$$[S] = \begin{bmatrix} \frac{1}{E_1} & -\frac{\nu_{12}}{E_1} & 0 \\ -\frac{\nu_{21}}{E_2} & \frac{1}{E_2} & 0 \\ 0 & 0 & \frac{1}{G_{12}} \end{bmatrix} \tag{2}$$

where, E_1,E_2,G_{12},ν_{12} and ν_{21} are Young's moduli, shear moduli and Poisson's ratios in principal material directions, respectively.

Based on the compliance matrix $[S]$, the reduced stiffness matrix $[Q]$ in principal material directions is given as

$$[Q] = [S]^{-1} \tag{3}$$

The matrices $[T_1(\theta)]$ and $[T_2(\theta)]$ are transformation matrices and are given as

$$[T_1(\theta)] = \begin{bmatrix} m^2 & n^2 & 2mn \\ n^2 & m^2 & -2mn \\ -mn & mn & m^2-n^2 \end{bmatrix} \quad [T_2(\theta)] = \begin{bmatrix} m^2 & n^2 & -mn \\ n^2 & m^2 & -mn \\ -2mn & 2mn & m^2-n^2 \end{bmatrix} \tag{4}$$

where, m, n are $cos\theta$ and $sin\theta$, respectively.

Now, based on transformation matrices $[T_1(\theta)]$ and $[T_2(\theta)]$, the transformed stiffness matrix $[\overline{Q}(\theta)]$ for lamina oriented at an angle θ with respect to global coordinate system can be written as,

$$[\overline{Q}(\theta)] = [T_1(\theta)]^{-1}[Q][T_2(\theta)] \tag{5}$$

In terms of lamina thickness and $[\overline{Q}(\theta)]$, the extensional stiffness matrix $[A]$ for laminate is,

$$[A] = \frac{1}{h}\sum_{k=1}^{n} [\overline{Q}(\theta_k)](t_k - t_{k-1}) \tag{6}$$

where, t_k and t_{k-1} are the k^{th} lamina top and bottom co-ordinates from the mid-plane and h is the total thickness of laminate. Now, the compliance matrix $[S]_{laminate}$ of a laminate is defined as (see Herakovich [30]),

$$[S]_{laminate} = [A]^{-1} \tag{7}$$

Using Eq. (7) and mechanical properties in Table 2, quasi-isotropic laminate mechanical properties of laminates were calculated. The percentage difference in elastic modulus and shear modulus of quasi-isotropic laminates are of the order of 20%. Therefore, metallic material is replaced by 1.2 times of CFC material with $\triangle\theta = 45°$ as preferred industrial choice for ply orientations in multiples of 4. The structural design details obtained as an initial size [27] of laminates formed after changing material are shown in Table 3. Thus, for example, the stiffener laminate will have $\frac{14.4}{0.15} = 96$ number of layers of 0.15 mm thickness each. Likewise, spar flange, spar web and stiffeners will have 120, 72 and 84 layers, respectively.

Table 2
Lamina properties IM7 [31].

Thickness	0.15 mm
E_1	163 GPa
E_2	12 GPa
G_{12}	6.3 GPa
ν_{12}	0.3

Table 3
Initial size of Metallic and Laminated WTB.

Element	Metallic Structure (mm)	Laminated Structure (mm)	No. of Layers
Top/Bottom panel thickness	12 to 3 tapering	14.4 to 3.6	96
Width of torsion box at root	1670	1670	
Mean height	314.0	314.0	
Rib pitch	360.0	360.0	
Spar flange thickness	15.0	18.0	120
Spar web thickness	9.0	10.8	72
Rib thickness	2.0	2.4	
Stiffeners (11 Nos.) thickness	10.5	12.6	84
Stiffener pitch	105	105	

4. GA optimization

In this section various aspects of GA optimization followed by Tsai-Wu first ply failure criterion used are discussed.

4.1. String (chromosomes) and design variables

The string of GA optimization contains information about the orientations and thickness (i.e., dummy or real ply) of each ply. A 12-layer symmetric laminate along with its equivalent string is depicted in Fig. 2. The length of any such unsymmetric laminate string is two times the number of plies in a laminate. To reduce the number of variables in the problem, the individual laminate is considered to be symmetric laminate in present problem as well as they are mirror images in sets of top/bottom and front/rear laminates for structural members of the WTB. For example, in this arrangement the top panel and bottom panel laminates are symmetric laminates on individual basis and also they are mirror images of each other as shown in sectional view of the wing along the span (see Fig. 3a). In this arrangement, even with the deletion of plies during automated optimization procedure the symmetry, taper and smoothness of top surface is maintained. The users can have separate laminates with independent sets of strings (with double length) without making replica of laminates for better optimized outcome. However, it will increase the computational time.

The strings for the optimization problem comprise of set of ply orientation and thickness. The orientation angle c_i can take 0°, ± 45° and 90° and thickness TH_i can have either 0 or 1 value, where 0 value is equivalent to 0.001 mm thickness and 1 value is equivalent to 0.15 mm thickness of the ply. The 0.001 mm value for thickness is equivalent to absence of a particular ply in the laminate. Such a layer is termed as dummy layer. Since, a zero thickness can not be assigned in a numerical analysis; therefore, a small thickness is given to the lamina.

It is to be noted that the industry preferred designs mostly contain symmetric laminates. Therefore, in the present problem the laminates are made symmetric. This reduces the number of design variables in a laminate by a factor of half. For each ply there are 4 possibilities of ply orientations (c_i) and two possibilities of ply thickness (TH_i) as mentioned above. Thus, there are $[48^4 * 48^2]$ number of laminate design possibilities for the panel. The same is elucidated in Fig. 2 in terms of bits used in strings of GA. In a similar way, the number of laminate design possibilities for flange spar, flange web and stiffeners are calculated. Thus, the problem size with feasible design variables will be $[48^4 * 48^2] * [60^4 * 60^2] * [36^4 * 36^2] * [42^4 * 42^2]$, i.e., 1.6e47 possible outcomes. This indicates a huge search domain for GA to work upon.

The algorithm developed for the current optimization problem is based on Elitist native search of non-dominated strings only as FE

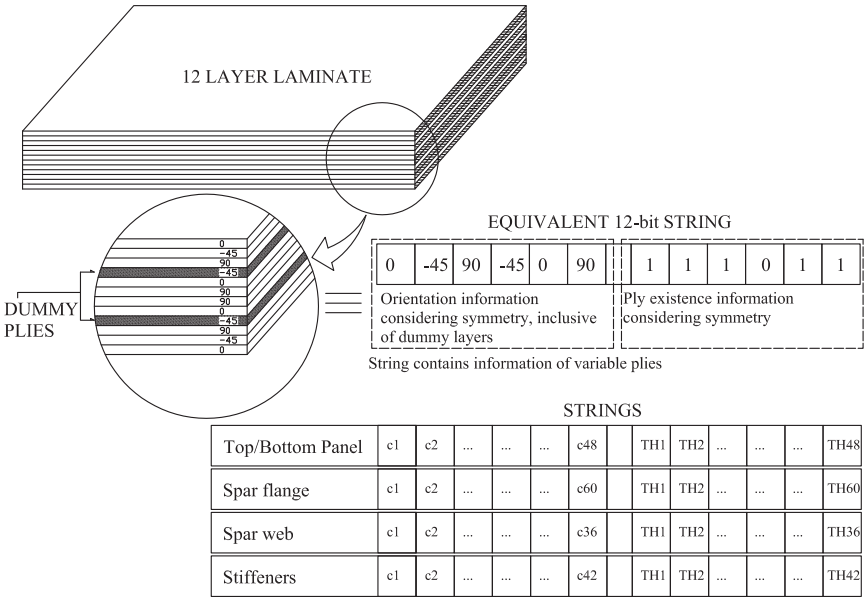

Fig. 2. Chromosomes representing equivalent laminates.

solution the problem takes 99% of computational time. Also once the string is submitted to FE solver, all three design objectives are simultaneously evaluated. Therefore, complexities discussed in [16] have minimal influence on total solution time. Based on the technique discussed in [9], the search efficiency of present problem may marginally improve for the solution time and search of optimal solution. However, this possibility can be explored as future scope to the current study.

4.2. Material axes

The material axis *M* along with its normal direction *N*, for different laminates is shown in Fig. 3b. In this study, we have preferably assigned the material axis in the direction of elastic axis so that the bending load directly gets transferred through 0° orientated plies. Therefore, the material axes for panels, spar-webs and spar-flanges are along the wing elastic axis but material axis for ribs and stiffeners is set along the global *z*-direction.

4.3. Finite element model of CFC wing for GA optimization

The model obtained after initial sizing has been used for the demonstration of the proposed GA optimization procedure. The FE model has been developed in ABAQUS/CAE with 5689 number of S4 4-noded doubly curved general purpose shell elements and 39 numbers of S3 3-noded general purpose shell elements. The elements used are finite strain shell elements with reduced integration scheme. The elements have displacements and rotational degrees of freedom and are well suited for modeling 3D structures for static as well as dynamic analyses. The shell section integrated during the analysis allows the cross-sectional behaviour to be calculated by numerical integration through the shell thickness. Thus, it provides complete generality in material modeling. Therefore, the section definition requires shell thickness, material and orientation of each layer. The element also allows transverse shear deformation, which is computed by matching the shear response of the shell to that of a three-dimensional solid for the case of bending about one axis. For composite shells, the transverse shear stiffness is defined as

$$K_{11}^{ts} = \frac{5}{6} * G_{13} * t,\ K_{22}^{ts} = \frac{5}{6} * G_{23} * t,\ K_{12}^{ts} = 0 \tag{8}$$

where, K_{ij}^{ts} are the shell section transverse stiffnesses, G_{13} and G_{23} are shear moduli in out of plane directions. The number $\frac{5}{6}$ is shear correction factor used for matching transverse shear energy in pure bending [32]. The mesh generated using S4 and S3 ABAQUS/CAE elements was a representative global wing mesh. The meshed model is analysed using ABAQUS/CAE on a 6 core CPU, 16 GB RAM mid-range workstation. The

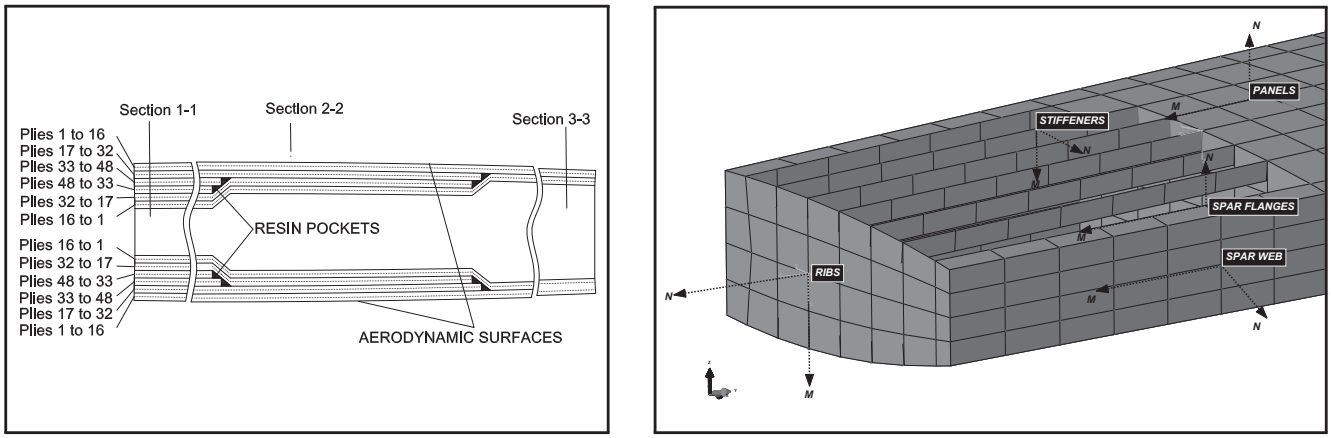

(a) (b)

Fig. 3. Ply arrangement (a) Top and bottom panel laminae arrangement (b) Material axis and normal direction.

Table 4
Interface python-script for panel *OPTIMIZER*.

```
import section                                                          # import ABAQUS environment
execfile('…/inputP.py')                                                 # import parametric values from another
                                                                        script written by MATLAB while optimization
p1  = mdb.models['Job-1'].parts['PART-1']                               # read job in CAE file
plySystem1  = mdb.models['Job-1'].parts['PART-1'].datums[45]            # read lamination details
…
plySystem48  = mdb.models['Job-1'].parts['PART-1'].datums[45]           # read lamination details
p  = mdb.models['Job-1'].parts['PART-1']                                # read laminate element set
region1 = p.sets['SEG1C-1']                                             # read region 1 details
…
region48 = p.sets['SEG1C-1']                                            # read region 48 details
compositeLayup  = mdb.models['Job-1'].parts['PART-1']. …                # define layup
compositeLayups['SEG1C']compositeLayup.orientation.setValues …
(additionalRotationType = ROTATION·NONE, angle = 0.0) …
compositeLayup.CompositePly(suppressed = False, …
plyName = 'PLY-1', region = region1,
material = 'IM-7', thicknessType = SPECIFY·THICKNESS, thickness = TH1, …   # update thickness variable TH1
orientationType = CSYS, orientation = plySystem1, axis = AXIS·3, …
angle = c1, additionalRotationField = '', additionalRotationType = …)   # update angle variable c1
ROTATION·ANGLE, numIntPoints = 3
…
compositeLayup  = mdb.models['Job-1'].parts['PART-1']. …
compositeLayups['SEG1C']compositeLayup.orientation.setValues …
(additionalRotationType = ROTATION·NONE, angle = 0.0) …
compositeLayup.CompositePly(suppressed = False, …
plyName = 'PLY-1', region = region1,
material = 'IM-7', thicknessType = SPECIFY·THICKNESS, thickness = TH48, …  # update thickness variable TH48
orientationType = CSYS, orientation = plySystem1, axis = AXIS·3, …
angle = c48, additionalRotationField = '', additionalRotationType = …)  # update angle variable c48
ROTATION·ANGLE, numIntPoints = 3
a  = mdb.models['Job-1'].rootAssembly
mdb.jobs['LAMINATED'].submit(consistencyChecking = OFF)                 # submission to solver
mdb.jobs['LAMINATED'].waitForCompletion()                               # wait for completion
o3  = session.openOdb('name = …/LAMINATED.odb')                         # start result session
odb  = session.odbs['…/LAMINATED.odb']                                  # open result file
session.fieldReportOptions.setValues(printXYData = OFF, printTotal = OFF)   # setting of report format
session.writeFieldReport(fileName = 'D:/…/abq-report.txt', append = OFF,    # write report file
sortItem = 'Node Label', odb = odb, step = 0, frame = 1, outputPosition = NODAL, …
variable = (('U', NODAL, ((INVARIANT, 'Magnitude'),)), ('SDV1', …
INTEGRATION·POINT),))
mdb.save(), sys.exit()                                                  # save and exit
```

laminates shown in Fig. 2 are defined in ABAQUS/CAE Laminate-Modeller (LM), where the ply orientation and thickness values are assigned. The boundary condition to FE model is defined as in-plane DOF constraints to panel nodes and all DOF translation constraint for spar web nodes at root.

The ply orientation c_i and thickness TH_i defined in LM are externally accessible in MATLAB by python-script. To generate such scripts, users have to start recording session of ABAQUS/CAE. During recording session, the commands given in GUI gets recorded to the python-script, within recording session if user alters design variable value, it also gets recorded to python-script file. The recorded python-script can be later linked to interactively update the design variable(s). For present problem the design variables are ply orientation c_i and lamina thickness TH_i. A representative python-script used for interface of panel optimization is given in Table 4. During optimization, the MATLAB based GA optimizer generates strings and updates the script file. The updated script file submits the FE problem to the solver with updated values of design variables for the evaluation of fitness function. On completion of the FE solution, the output of the ABAQUS/CAE is written to a ABAQUS report file, which is read by MATLAB algorithm to evaluate fitness function to guide the optimization procedure. The working of the python script is depicted in Fig. 4.

4.4. Fitness function

The fitness function Z for the present multi-objective multi-laminate wing optimization is expressed as

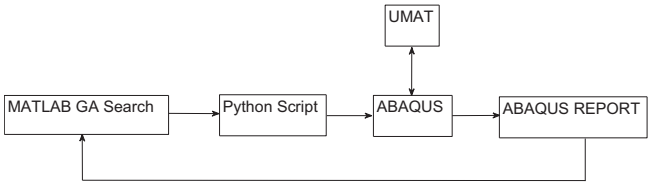

Fig. 4. Data flow during optimization.

$$\text{Minimize } (Z) = f_1 * w_1 + f_2 * w_2 + f_3 * w_3 \tag{9}$$

Subjected to design requirements

$$\begin{aligned} f_1 &= (FI - 1.0) * s_{fi} && \text{when } FI \geqslant 0 \\ f_1 &= 0 && \text{if } \quad FI < 0 \\ f_2 &= (D - D_a) * s_{def} && \text{when } D \geqslant D_a \\ f_2 &= 0 && \text{when } D < D_a \\ f_3 &= T_w * s_{tw} \end{aligned}$$

where, FI is Tsai-Wu first ply FI, D is wing tip deflection, D_a is maximum allowed wing tip deflection, T_w is total weight of structure and s_{fi}, s_{def} and s_{tw} are scaling factors over FI, D and T_w, respectively. The design criterion f_1 is for the static strength penalty. The structure is considered safe when the value of FI is less than 1. However, when FI is more than one, the structure is unsafe and therefore, f_1 imposes a penalty over the fitness function. The definition of f_1 is such that, the FI has to be within design allowable limits. However, it should be noted that the minimization of FI value is not required. Similarly, the design criterion f_2 is

for stiffness penalty. The f_2 function imposes penalty over the fitness function when D exceeds allowable value. In a similar way, f_2 also need not to be minimized but its value should be within specified design limits. The f_3 function is directly the weight of assembly which has to be minimized. These requirements are connected in the form of a fitness function given in Eq. (9). It is noteworthy that during optimization when FI and D are within design limits, the fitness function remains as a pure function of assembly weight. However, when there is deviation of FI and D from allowable design values, the functions f_1 and f_2 impose penalties over the fitness function Z. Therefore, the function does not remain minimal. This approach is termed as penalty approach and was used by Srinivas and Deb [33] and Ball et al. [34] in different forms.

The objective functions have different maximum allowable values. Thus, when they are used to form a fitness function they must be brought to a common level. Therefore, these functions are scaled. The scaling factors normalizes the design variables [35] in fitness function, which can be decided based on nominal values of design variables as given in the following equation.

$$s(x_i) = \frac{max.(x_i) - min.(x_i)}{max.(x_c) - min.(x_c)} \tag{10}$$

To evaluate the scaling factors, designer can choose one of the design variable (x_c) as base variable and do the normalization of other variables. For present problem, scaling factors s_{fi} and s_{def} are calculated as 690 and 0.74, respectively on the basis of initial weight, T_w, of the structure. The influence of scaling factor has been brought out in Section 5.2. Apart from the scaling factors, weights w_i are incorporated in Eq. (9) to prioritize the importance of design variables. A systematic approach for the weight (w_i) selection is also discussed in Section 5.2.

4.5. GA operations

As the solution sequence proceeds, the strings exchange their bits in pieces to form new strings by doing crossover operations. The strings also participate in mutation to bring in new strings. However, crossover and mutations are within a certain set of guidelines to maintain consistency in strings. The following operations are part of the proposed GA process.

(a) The strings undergo bi-level crossover, in which exchange occurs simultaneously at two positions of the strings as shown in Fig. 5a. The bi-level crossover is defined to exchange string portion within the orientation/thickness domain(s). This brings in variety in terms of orientations and thicknesses simultaneously.
(b) Depending upon the value of FI, the mutation operator converts real plies to dummy plies for X% (mutation percentage) of plies and vice-a-versa.
(c) A X% mutation is also applicable to c_i, which brings in new strings in search domain as shown in Fig. 5b.
(d) Algorithm decides crossover and mutation sites by a random number generator.

4.6. Process flow

The classical GA optimization procedure for the present problem is based on generation of new strings by crossover and mutation. A detailed insight of GA operations is given in Fig. 6. Here, it can be seen that for generation of a mating pool, sorting of strings was done based on their fitness values. After sorting bottom half (poor quality) of the strings are rejected and replaced by new one after probabilistic (roulette wheel) selection [36]. Again, new strings are evaluated on FE solver for fitness value. The process flow of optimization algorithm is given in Fig. 7, in which the optimizer starts with a set of strings obtained after conversion of the structure from metallic to a quasi-isotropic laminate. The model with the assigned set of strings is evaluated for fitness value. As one of the function *OPTIMIZER* is called for the first time, the optimizer generates n random initial population string set, on which crossover and mutation are performed for searching an optimal set of string. After the end of GA operations, the population is evaluated for fitness value of each string based on Eq. (9). Now, solution goes to sub-loop *MR-LOOP*. Here, $n/2$ string sets with better fitness values are cloned and remaining $n/2$ string sets are replaced by new strings, which come from the first half parents after GA operations. When the *OPTIMIZER* is called for the subsequent time, it uses the sets of strings available from previously stored results as an initial population.

At the end of *OPTIMIZER* sub-loop, the results of FE solution are read by the algorithm to identify the laminate with *MFI*. The identified laminate is selected as next *OPTIMIZER* sub-loop for the process. Here, this methodology is termed as laminate selection strategy (LSS). The procedure is iterative in nature; therefore, at the end of every *OPTIMIZER* sub-loop, the laminate is identified for next step. The process is depicted in the algorithm of Table 5. The LSS breaks the sequential flow of algorithm to bring down computational time.

4.7. Failure criterion

The quadratic failure criterion was preferred for better approximation of the failures from strength aspect. The Tsai-Wu failure criterion [30] [37] given in Eq. (11) is used in the present study.

$$FI = \sigma_1\left(\frac{1}{X_t} - \frac{1}{X_c}\right) + \sigma_2\left(\frac{1}{Y_t} - \frac{1}{Y_c}\right) - \frac{\sigma_1^2}{X_t * X_c} - \frac{\sigma_2^2}{Y_t * Y_c} - \frac{\sigma_{12}^2}{S^2} \tag{11}$$

where, X, Y are the lamina strengths in x and y-directions, S is shear

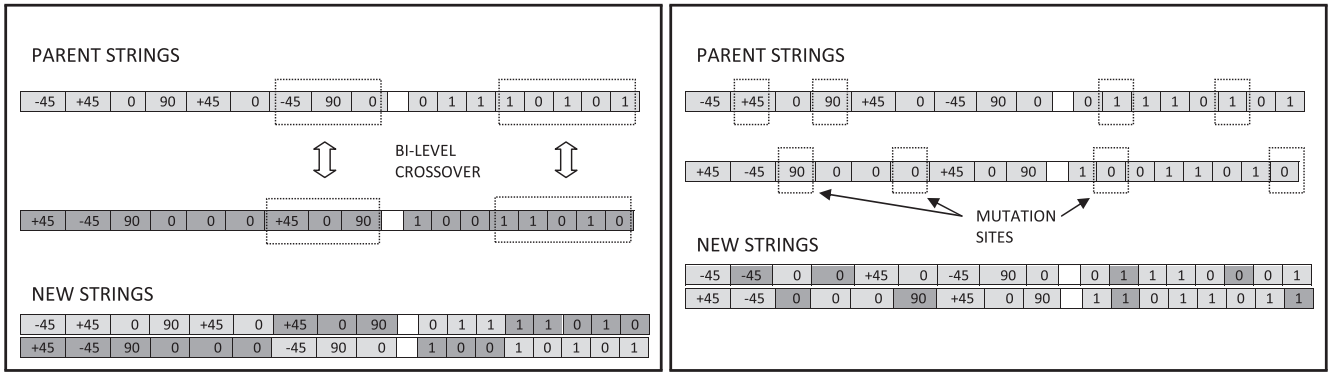

Fig. 5. GA operators (a) Bi-Level crossover (b) Mutation.

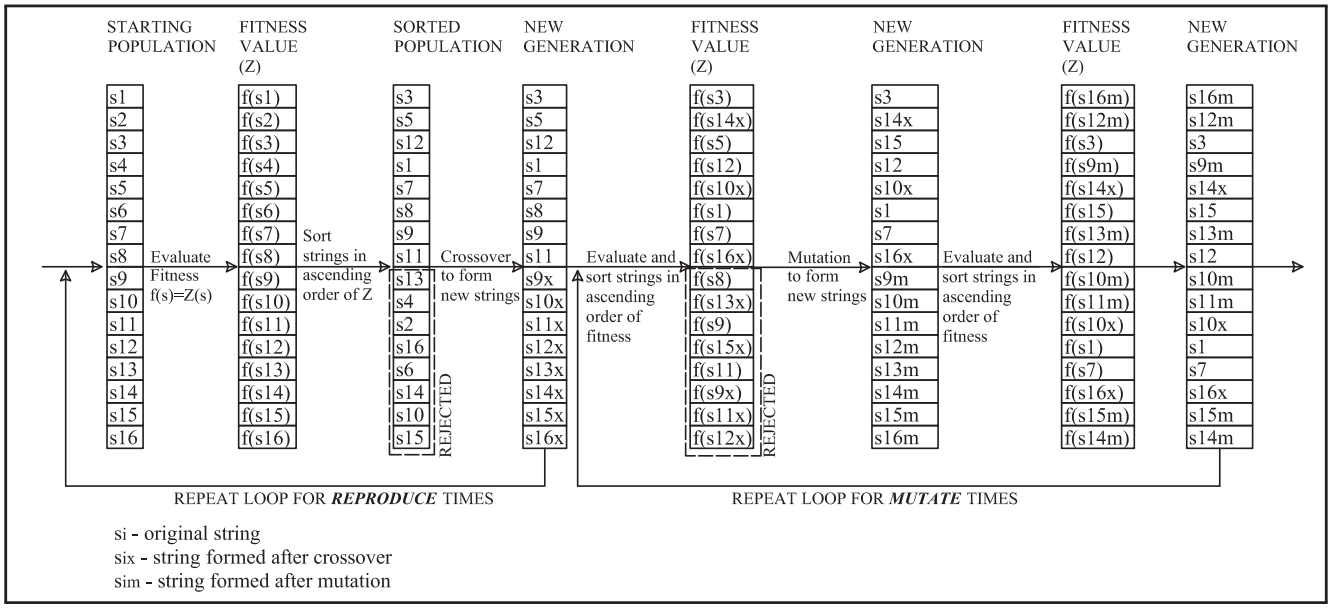

Fig. 6. Example showing working of GA operations.

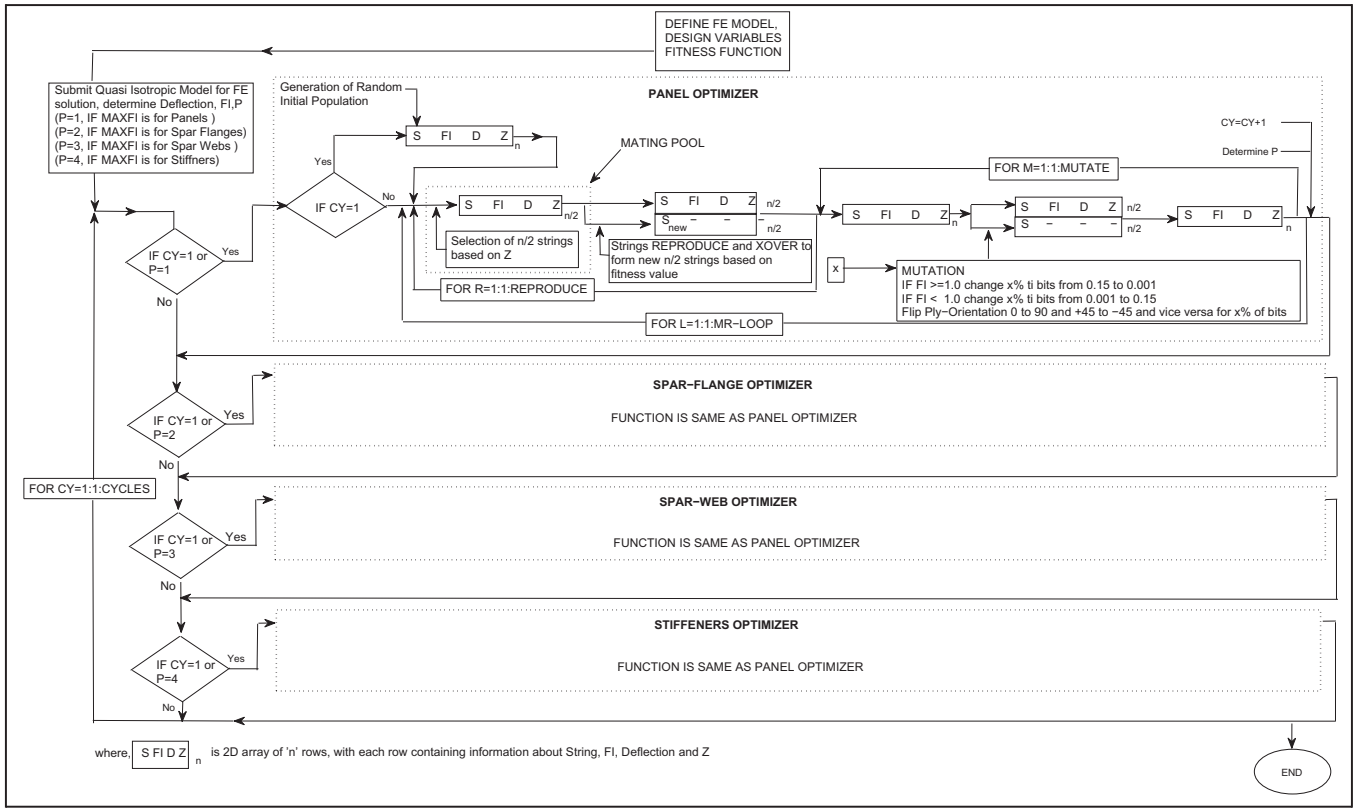

Fig. 7. GA Flow Diagram.

strength in *xy*-plane, respectively. The subscripts *t* and *c* denote tensile and compressive nature, respectively. The Tsai-Wu failure criterion is not directly available in ABAQUS/CAE; therefore, the failure criterion is defined for ABAQUS using UMAT and is given in Table 6.

Apart from the strength criterion, stiffness criterion as 10% of *D* is important for the wing design. To obtain a minimal weight for the optimized wing design, a satisfactory fulfilment of both strength and stiffness criteria is required, which is designed in the algorithm by Eq. (9).

5. Results and discussion

This section highlights the effect of conversion of real plies to dummy plies (0.001 mm thickness) within the laminates as discussed in Section 4.1 and results of GA optimization along with selection of weight factors, w_i. It also brings out the influence of scaling factor on solution convergence. Further, this section presents a comparison between behaviour of GA optimized FE model (which may include dummy plies) and a FE model developed using a laminate obtained from GA optimized solution with the dummy plies removed. The FE

Table 5
Laminate selection algorithm for optimization.

```
DO CY = 1,CYCLES
P = 1 (IF MFI is at PANELS)
P = 2 (IF MFI is at FLANGES)
P = 3 (IF MFI is at WEBS)
P = 4 (IF MFI is at STIFFENERS)
IF P = 1 OR CY = 1 OR FI<1.0; PANEL OPTIMIZE; UPDATE P;
IF P = 2 OR CY = 1 OR FI<1.0; FLANGE OPTIMIZE; UPDATE P;
IF P = 3 OR CY = 1 OR FI<1.0; WEB OPTIMIZE; UPDATE P;
IF P = 4 OR CY = 1 OR FI<1.0; STIFFENER OPTIMIZE; UPDATE P;
ENDFOR
```

Table 6
UMAT for Tsai-Wu FI evaluation.

TSAIWU(E_1,E_2,Nu_{12},Nu_{23},G_{12},X_t,X_c,Y_t,Y_c,S,*FI*)
EVALUATION OF TOTAL STRAIN
DO I = 1,3; STRAN(I) = STRAN(I) + DSTRAN(I); END DO
CALL LMMSTIFF(PROPS,NPROPS,XLMSTIFF)
CALL MULTI(XLMSTIFF,STRAN,STRESS)
DO I = 1,3; DO J = 1,3; DDSDDE (I,J) = XLMSTIFF (I,J); END DO; END DO; RETURN; END
EVALUATION OF STIFFNESS MATRIX
XLMSTIFF(1,1) = $E1/(1.0-Nu_{12} * Nu_{21})$,
XLMSTIFF(1,2) = $(Nu_{12} * E2)/(1.0-Nu_{12} * Nu_{21})$
XLMSTIFF(2,1) = XLMSTIFF(1,2); XLMSTIFF(2,2) = $E2/(1.0-Nu_{12} * Nu_{21})$;
XLMSTIFF(3,3) = G_{12};
EVALUATION OF FAILURE INDEX
FI = STRESS(1,1) * $(1/X_t)$ + $(1/X_c)$ + STRESS(1,2) * $((1/Y_t)+(1/Y_c))$ − (STRESS $(1,1)^2/(X_t * X_c)$) − …
$(STRESS(1,2)^2/(Y_t * Y_c))$ + $(STRESS(1,3)^2/S^2)$

Table 7
Comparison of FE output for thickness change.

Laminate	Laminate Details	*FI*	Deflection (mm)
L1 $[0/45/(90)_2/45/0]_S$	12 plies of 0.15 mm each	4.20e-3	23.14 mm
L2 $[0/45/(90)_2/45/(0)_2/45/90]_S$	18 plies of 0.15 mm each	1.05e-3	15.01 mm
L3 $[0/45/(90)_2/45/(0)_2/45/90]_S$	12 outer plies of 0.15 mm and 6 central plies of 0.001 mm	4.16e-3	23.05 mm

model obtained is verified for buckling check as well and the final solution is presented with readjusted laminates. Lastly, the effect of mutation percentage on convergence is presented.

5.1. Conversion of real plies to dummy plies within a laminate

To optimize structural weight, conversion of a real layer into a dummy layer in laminates is required. In an automated process whenever a ply is deleted the FE model definition is changed. To avoid this, we have introduced the concept of conversion of real plies to dummy plies during solution sequence. The introduction of a dummy ply in the model is studied by analytic experiments of assigning a near zero thickness value (0.001 mm) to plies.

In analytic experiments, three laminates (L1, L2 and L3) have been considered as given in Table 7. The laminates are of 100 × 10 mm size and are subjected to unit loading at one end in normal and longitudinal directions of the laminate, while other end is rigidly fixed. The laminate L1 consists of 12 layers and L2 consists of 18 layers with 0.15 mm thickness each. The outer 12 layers in L2 have same orientation except the middle 6 layers. The laminate L3 consists of 18 layers, with same orientation as in L2, but middle 6 layers have a thickness of 0.001 mm each. Thus, the laminate L1 and L3 are equivalent in orientations and thicknesses.

These laminates are then analysed for deflection with *FI* within the limit. These values are also reported in Table 7. The deflection outputs from the analyses for three laminates have been compared. It can be seen that the deflections of L1 and L3 are comparable with less than 0.5% difference. The close match in results of L1 and L3 laminate indicates that the laminate of 18 layers with 6 layers of near zero ply thickness is equivalent to 12 layers laminate in overall behaviour as well. Further, there is no spurious behaviour in FE results with the introduction of 0.001 mm thickness plies in the laminate (see Fig. 8). Therefore, it is possible to do removal of plies in an automated manner by introducing dummy layers.

Thus, this analytic experiment clearly demonstrates the concept of conversion of real plies to dummy plies without any loss of overall behaviour in the model.

5.2. GA optimization

The solution to the optimization problem considered is started with an initial metallic design where the structural weight was 1100.4 kg. The metallic structure is converted to an equivalent quasi-isotropic laminated structure, with the strength parameters of commercially available UD carbon pre-pregs of IM7/8552 [31]. This is a high performance tough epoxy matrix system for primary usage in aerospace structures. The quasi-isotropic laminated structure with the weight of 690 kg was submitted to GA optimizer with solution parameters as $X = 10\%$, $n = 16$, $MR\text{-}LOOP = 2$, REPRODUCE = 2, D_a = 927 mm and w_i as per Table 8. The weight vector selection for optimal results was based on the series of solutions (a posteriori articulation) with different w_i as given in Table 8. The solution to different cases of w_i is submitted to solver and the resulting values of FI, D and T_w are also given are Table 8.

In Table 8, the first three cases deal with the weights such that only one objective function is active with the corresponding weight of 1. Thus, Case 1 and Case 2 have only strength and stiffness (*FI* and *D*) functions active, respectively. For Case 3, only structural weight (T_w) function is active. The solutions to Case 1 and Case 2 had pre-matured termination as algorithm was unable to do selection of strings for

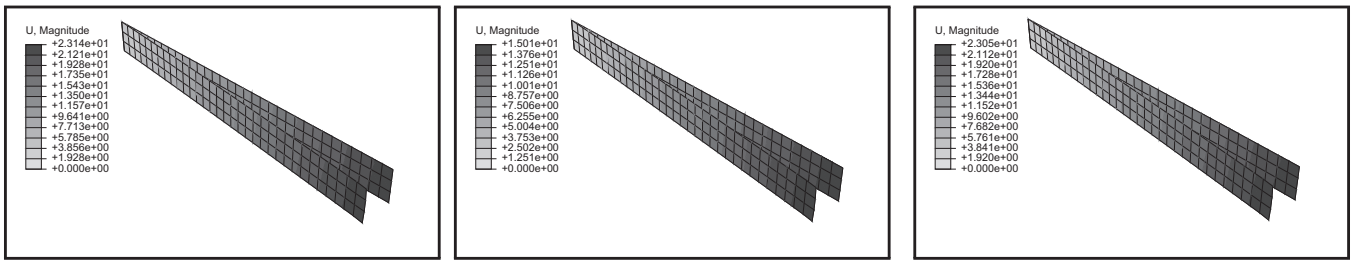

(a) (b) (c)

Fig. 8. Laminate deflection (mm) (a) L1 (b) L2 (c) L3.

Table 8
Optimized Results with w_i choices.

Case No.	w_i	*FI*	Def. (mm)	Total weight (kg)	Remarks
1.	(1,0,0)	0.94	809	636	Pre-matured run termination
2.	(0,1,0)	0.96	830	690	Pre-matured run termination
3.	(0,0,1)	1.62	1130	467	Design allowable exceeded
4.	$\left(\frac{1}{2},\frac{1}{2},0\right)$	0.87	792	630	No significant weight reduction
5.	$\left(\frac{1}{2},0,\frac{1}{2}\right)$	0.99	999	416	Allowable *D* exceeded
6.	$\left(0,\frac{1}{2},\frac{1}{2}\right)$	1.08	914	528	Allowable *FI* exceeded
7.	$\left(\frac{1}{3},\frac{1}{3},\frac{1}{3}\right)$	1.00	1015	550	Design allowable exceeded
8.	$\left(\frac{3}{8},\frac{3}{8},\frac{2}{8}\right)$	0.99	919	499	Acceptable Solution
9.	$\left(\frac{4}{10},\frac{4}{10},\frac{2}{10}\right)$	1.00	924	485	Acceptable Solution
10.	$\left(\frac{5}{12},\frac{5}{12},\frac{2}{12}\right)$	0.99	923	476	Acceptable Solution
11.	$\left(\frac{1}{2},\frac{1}{3},\frac{1}{6}\right)$	0.99	869	489	Acceptable Solution
12.	$\left(\frac{1}{3},\frac{1}{2},\frac{1}{6}\right)$	0.90	818	543	Acceptable Solution
13.	$\left(\frac{1}{10},\frac{1}{10},\frac{8}{10}\right)$	1.08	954	489	Design allowable exceeded

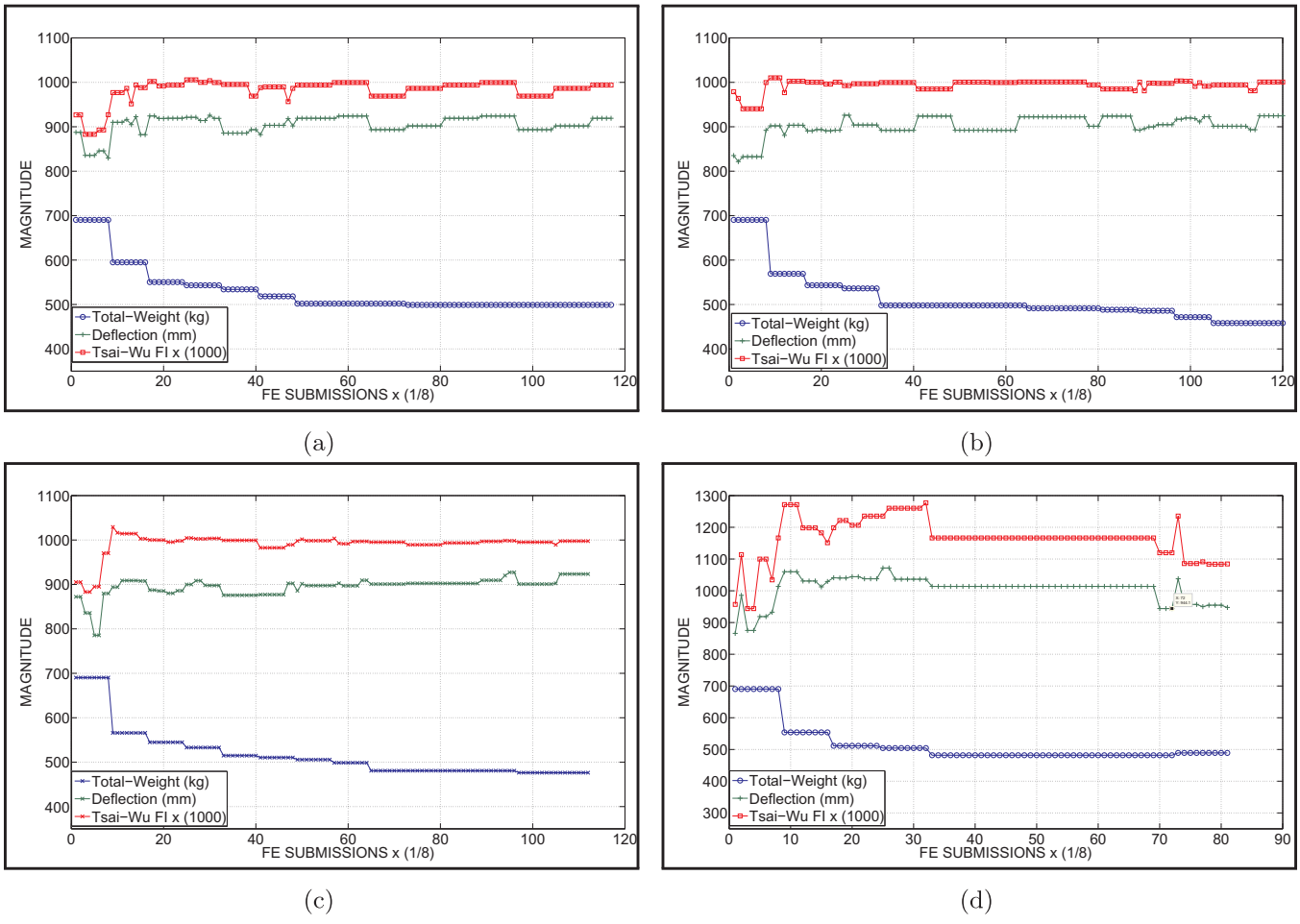

Fig. 9. Convergence plots (a) Case 8, (b) Case 9, (c) Case 10, (d) Case 13.

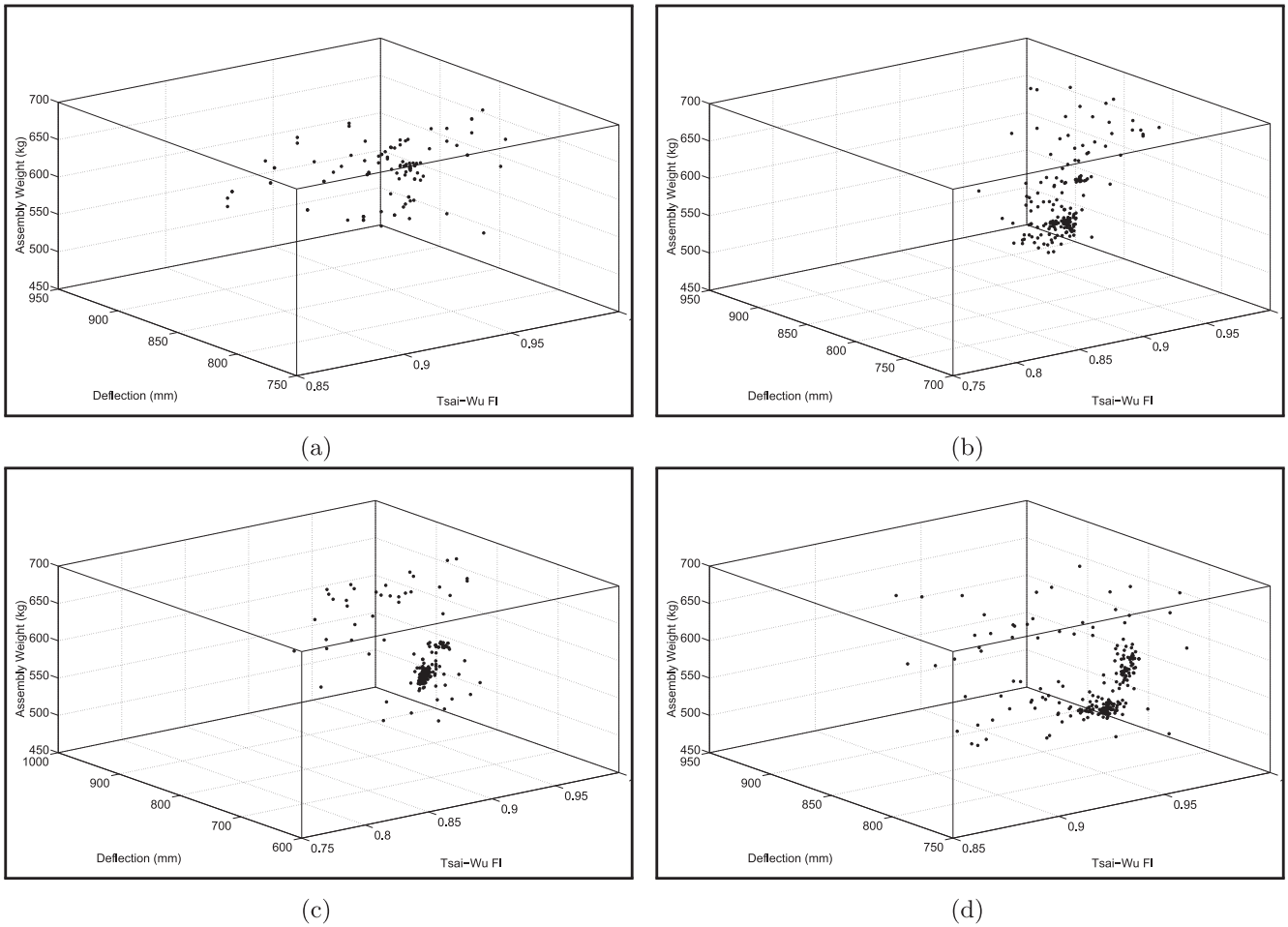

Fig. 10. Data Points in 3D space for (a) Case 8, (b) Case 9, (c) Case 10, (d) Case 11.

crossover. This is because all the strings have same (zero) value of fitness function Z after few iterations. In Case 3, the solution is completed and there is a weight reduction but at the cost of violation of design requirements. In this case, the objective function Z becomes purely a function of T_w and it has no control over the values of FI and T_w.

The next three cases have only two out of three functions given equal weights of 0.5. For Case 4 only FI and D functions are active, for Case 5 FI and T_w functions are active and for Case 6 D and T_w are active. The results show that the Case 4 has no significant weight reduction as objective function was independent of T_w. In Case 5, allowable D value is exceeded as optimization is only between FI and T_w, irrespective of D. This behaviour is like a single-objective optimization problem. The Case 6 also behaved as single objective optimization to optimize with respect to D at the cost of FI. However, the Case 7, having equal priority for all the functions, showed design failure. The reason for this behaviour is that in this case the fitness function failed to understand that it has to bring down T_w only after maintaining the FI and D values within design limits. However, it has treated all design requirements with equal priority as assigned.

Solutions for the Case 8 through Case 12 are acceptable. For these cases w_1 and w_2 are higher than w_3, which indicates a *design-rule* over the fitness function. The *design rule* for present design is: 'minimize weight only when FI and D design variable values are within allowable design limits'. This indicates that the choices of w_i are governed on design requirements, which can be adjusted by users to their design choices as a posteriori articulation by weighted sum method [35,38]. Out of the acceptable Cases 8–12, the Case 9, Case 10 and Case 11 are comparable with minimum T_w, however Case 11 is better over the Case 9 and Case 10 as it has better design margins, therefore the Case 11 weight factors are selected as a design choice. The last case, Case 13 is equivalent to Case 3, in which design variables got exceeded while optimization. The convergence plots, data scatter, Pareto front for some of the important cases of Table 8 are given in Figs. 9, 10 and 11, respectively.

The convex hull plots by MATLAB post-processing of 3D scatter data are given in Fig. 11. The front obtained by the hull plot is Pareto front of subject 3D problem, which is formed by joining of the outer points (P_1....P_n) of feasible solutions cloud. It can be noted that the front obtained is essentially a convex front emerging from the bottom most point on the plane parallel to FI and D axes. The emerging of Pareto front from single point confirms the fitness function to be a convex objective function, therefore this makes it suitable for a posteriori articulation.

To study influence of the scaling factors on results, solution has been submitted with unity value of s_{fi}, s_{def} and s_{tw}. By making scaling factors as unity, the contribution of FI towards fitness function became negligible. Therefore, the convergence plot of Fig. 12 showed that FI design variable violated allowable design limit as the solution iterates.

The monitoring of solution convergence and laminate weights for Case 11 are given in Fig. 13. The Fig. 13a shows that T_w design variable has typical *hill-climbing* behaviour as desired, which is continuously reducing from the starting of iterations till the end. Moreover, it can be seen from Fig. 13a that FI and D are stabilized near to their design values. After about 880 FE submissions the solution is stabilized and accepted as an optimal solution. At this stage, the optimized solution has 201 kg lesser weight as compared to starting quasi-isotropic structure weight. However, the final weight of the structure may be marginally higher after buckling check, which is discussed in Section 5.4.

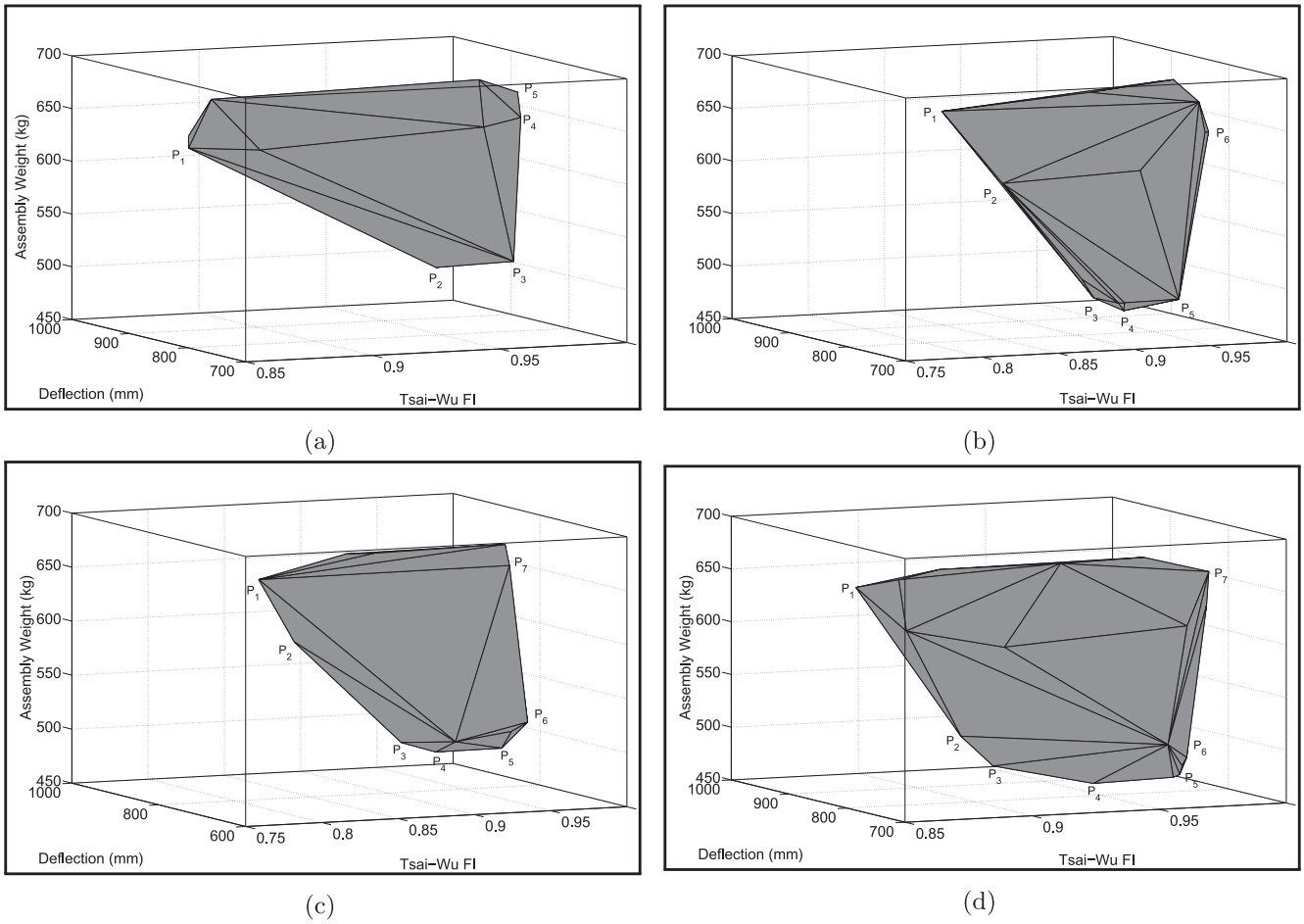

Fig. 11. Pareto front for (a) Case 8, (b) Case 9, (c) Case 10, (d) Case 11.

The Fig. 13b shows weight reduction at different laminates during optimization. The initial weight drop sequence was panel, flange, stiffener, flange, web and so on. However, in the next iteration this sequence is altered by LSS.

5.3. Verification of optimal solution

In this section the optimized solution given by the optimizer is modeled again without considering the dummy plies. Its FE analysis is done and compared with optimized solution. This verification is similar to the analytic experiment carried out earlier.

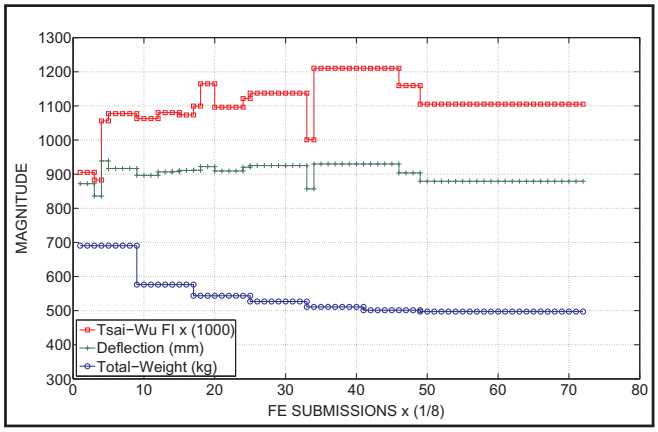

Fig. 12. Monitoring of design variables (Case 11) without normalization.

The Table 9 shows orientation and thickness of plies for the laminates obtained by employing GA optimization. The subscript *1* to the orientation indicates presence of a ply of 0.15 mm thickness. The subscript *0* indicates a dummy ply in the laminate. However, one can see the subscript *1* for the plies in the rib laminates as they were not part of optimization. The verification of the outcome of GA optimizer has been done by manually entering the lamination details (without dummy plies) of Table 9 to a FE model. The *D* and *FI* from the FE solution plots are given in Fig. 14. The results of comparison of convergence (Fig. 13) with FE analysis results (Fig. 14) are reported in Table 10. The table clearly shows that both results are comparable with a maximum difference of 2% in the *FI*. However, these small differences are due to reading of results at centroid of element and Gauss point by optimizer and FE solution, respectively. Furthermore, it must be noted that the difference in the overall structural weight was due to the geometric approximations made for the airfoil curvature.

5.4. Buckling check

The buckling analysis of the optimized model becomes essential at this stage as almost 28% of plies have been deleted during optimization. Furthermore, the panels and ribs are thin and their design based on buckling criterion is also important. However, this has not been implemented explicitly in the present optimization study to keep the level of complexity at a manageable level.

Here, a separate buckling analysis of the optimized solution has been carried out. The buckling plots of the initial critical modes are shown in Fig. 15. The initial buckling mode is on ribs and has an eigenvalue of 0.84. It means that the ribs are weak from buckling aspect.

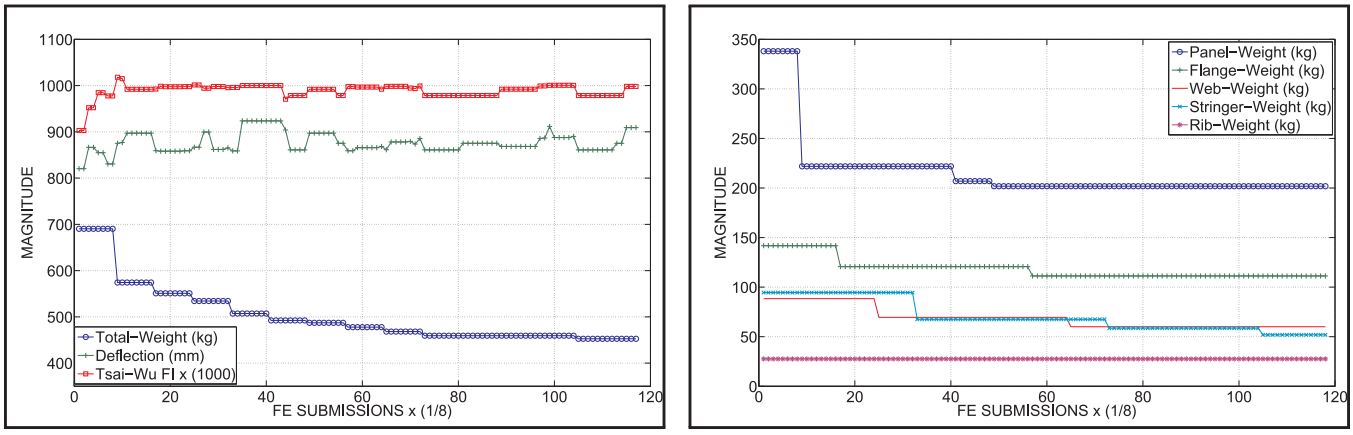

Fig. 13. Case 11, i.e., w_i = (0.5,0.3334,0.1667) (a) Convergence Plot, (b) Weight Optimization.

Table 9
Ply orientation and thickness output by optimizer after optimization for symmetric laminates

Panels: $90_1/90_1/0_0/0_1/135_0/0_0/45_1/0_1/135_1/90_0/90_1/45_0/0_1/90_0/0_1/0_1/0_1/90_0/0_1/0_1/0_0/0_1/90_0/90_0$
$/135_0/0_1/0_1/45_1/$
$135_1/0_1/90_1/90_0/0_1/45_1/90_1/90_1/0_0/45_1/0_1/45_1/90_1/90_1/0_1/135_1/0_1/45_0/0_1/0_0$

Spar Web: $135_1/135_1/45_0/45_1/135_1/135_1/0_1/135_1/0_1/0_1/90_0/45_0/45_1/45_1/0_1/135_1/90_1/45_1/0_0/90_1/135_1/0_1$
$/0_1/$
$135_1/90_0/0_0/135_1/90_1/45_1/90_0/90_1/135_1/135_0/45_0/135_1/0_0$

Spar Flange: $0_0/45_1/90_1/90_1/90_1/90_1/135_1/45_1/90_0/90_1/90_1/90_1/45_1/90_0/135_0/0_1/90_1/0_0/135_1/0_1/90_0/0_1/45_1$
$/90_1/0_1/90_1/$
$90_1/0_0/90_0/90_1/0_0/135_1/90_1/90_1/45_1/135_0/45_1/90_1/45_1/90_0/90_1/90_1/90_1/90_1/90_1/90_1/45_1/90_1/90_0$
$/135_1/90_1/45_0/90_1/0_1/0_0$
$/135_1/0_0/45_0/90_0/90_1/0_1/45_0$

Stiffeners: $0_1/0_0/0_0/0_1/90_0/45_1/0_1/0_1/0_1/0_1/0_1/135_0/0_1/0_1/90_1/0_1/0_1/45_1/45_1/135_1/135_1/90_1/0_1/90_0/0_0$
$/0_0/45_0/0_1/$
$0_1/0_0/45_1/90_0/135_1/0_1/45_1/0_1/0_1/0_1/0_1/135_1/0_0/135_1$

Ribs: $135_1/45_1/0_1/45_1/90_1/\text{-}45_1/0_1/45_1$

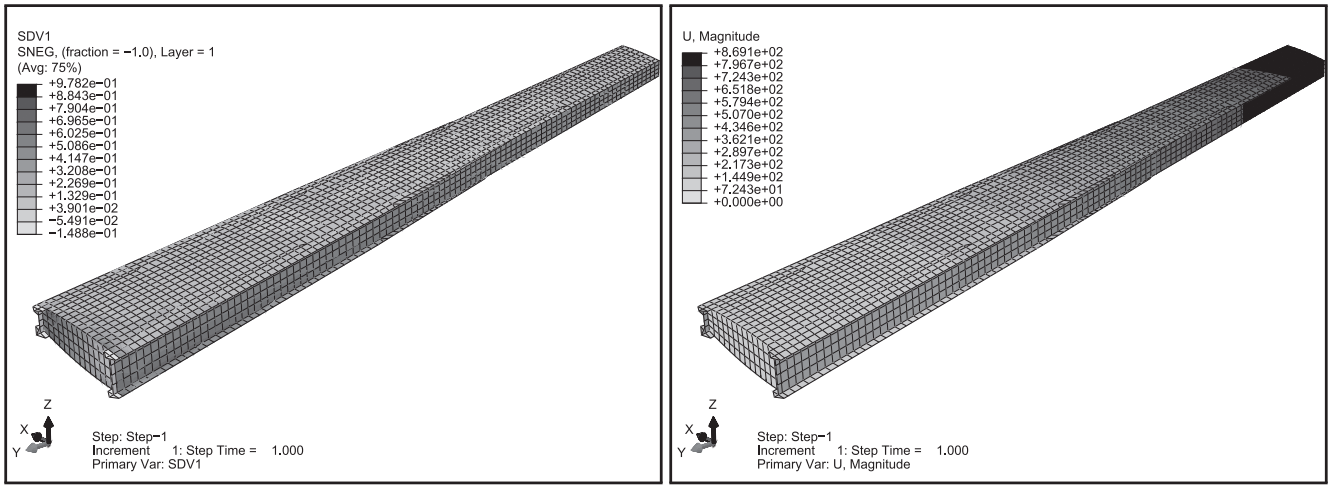

Fig. 14. FE analysis results of GA optimized model (a) Tsai-Wu FI distribution, (b) Deflection (mm) plot.

Table 10
Comparison of FE output with GA results

Parameter	GA Parameter (Fig. 13a)	FE Analysis of Table 9 laminates	% difference
First Ply FI	0.99	0.97	2.02
D (mm)	868.9	869.1	0.02
Weight (kg)	489.6	486.5	0.63

transfer torsional loads as well. Thus, this ply distribution in relation to the load bearing, as mentioned, is another good indicator that proposed GA works well.

5.6. Effect of mutation percentage

The mutation plays an important role to bring in variety in strings by altering the bits during GA optimization. A small study is carried out to determine the effect of mutation percentage on the optimization

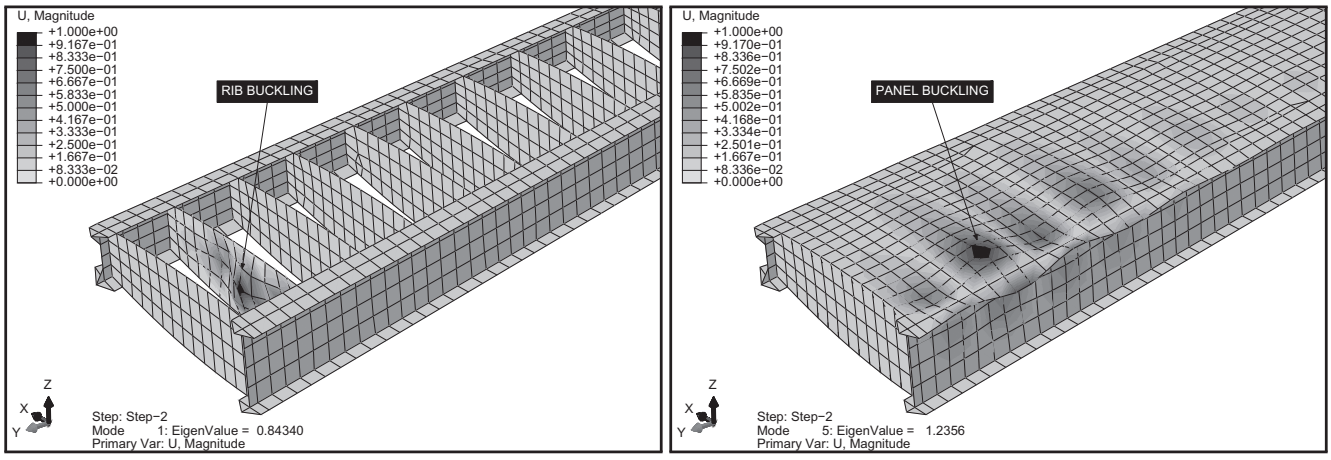

(a) (b)

Fig. 15. Buckling analysis modes (a) Initial modes (b) Higher modes.

Therefore, to strengthen the ribs against buckling, $[\pm 45]_2$ plies were added to the ribs laminates. The final laminates, formed after deleting near zero thickness plies; addition of plies for strengthening against buckling and readjustment of two plies so as to have ± 45 plies on the outer layer of laminate, are given in Table 11. The introduction of additional plies made the structure airworthy against buckling with the increase in weight from 489 kg to 501 kg, which is 2.5% of the total weight. The FE analysis results of laminated set of Table 11 are given in Fig. 16. It indicates that after optimization and necessary readjustment of some plies, the structure is safe from strength and buckling points of view, along with its D within the acceptable limit.

5.5. Ply distribution in optimal laminate

The ply distribution details of the readjusted laminae for the laminates in panels, spar webs and flanges and stiffeners are presented in Table 12. A closer look into the ply distribution indicates that the maximum number of plies acquire alignment along the loading direction. It is well known that the wing panels and stiffeners are predominantly loaded due to bending and they experience tension/compression load. Therefore, after optimization almost 50–60% plies get oriented with 0° direction in these laminates. Similarly, almost 60% plies of spar web adopted orientation of ± 45° as webs predominantly take care for shear load coming over the wing surface. However, spar flanges showed more plies in 90° orientation because they have to process. The plots for T_w with FI and D for different mutation percentage X for first 990 FE submissions are shown in Fig. 17. Introducing a small deviation (1%) in string-bits, brings in new strings with almost similar characteristics as of its parent. Therefore, solution is likely to stuck in local optima, which is evident in Fig. 17a. When mutation value is increased to 10% the convergence became faster (Ref. Fig. 17b). In this case, the solution searches global optima at a faster rate compared to previous case.

The larger values of mutation introduce major change in a string in single shot, which leads to loss of good characteristics of parent strings and therefore, formation of new good-strings becomes difficult. The situation is equivalent to *no-mutation* as most of the new strings formed in mutation got rejected. Therefore, the same set of parent strings keep on participating in crossover, due to which we see repeated patterns in Fig. 17c and d for FI and D plots. The situation is termed as premature convergence which can be recognized as *repeated-patterns* and can be avoided by the choice of moderate value of mutation.

Remark: The current study has been carried out for the most critical wing loading case. However, after small modifications to this algorithm, the optimizer can be used to optimally strengthen the structure for other/combined load cases as well. In that case, the optimizer may add plies to the structure to suffice for the D and first ply FI acceptability criteria as depicted by flow diagram in Fig. 18.

Table 11
Readjusted laminate details

Top/Bottom Panel	$[\pm 45/90_2/0_2/90/0_9/45/-45/0/90/0/45/90_2/45/0/45/90_2/0/-45/0/0]_S$
Spar Web	$[\pm 45/-45_3/0/-45/0_2/45_2/0/-45/90/45/90/-45/0_2/-45_2/90/45/90/-45_2]_S$
Spar Flange	$[\pm 45/90_4/\mp 45/90_2/45/0/90/-45/0_2/45/90/0/90_5/45_2/90/45/90_5/45/90/-45/90_2/0/-45/90/0]_S$
Stiffeners	$[\pm 45/0_9/90/0_2/45_2/-45/90/0_3/\pm 45/0/45/0_4/-45_2]_S$
Ribs	$[\pm 45_3/0/45/90/-45/0/45]_S$

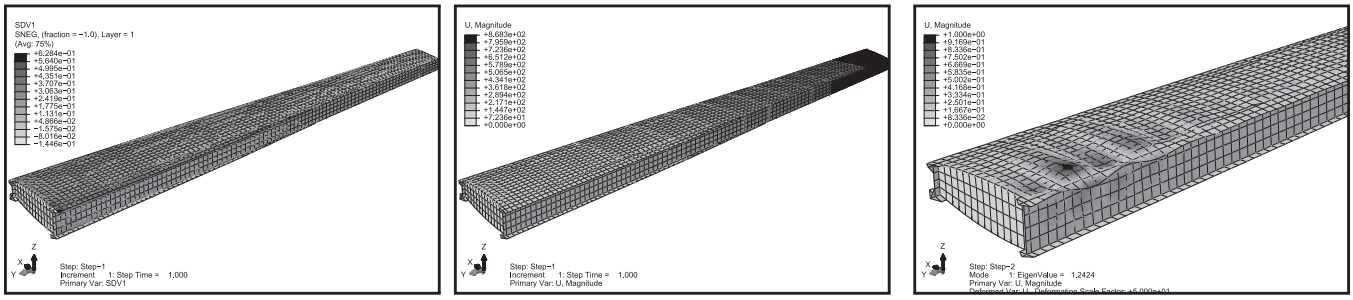

Fig. 16. Readjusted laminate analysis result plots (a) First ply FI (b) Deflection (mm) (c) Buckling mode.

Table 12
Ply orientation distribution of Plies in WTB Laminae

Orientation	0°	(90°	± 45°
Number (%) of Plies in Panels	34 (51)	16 (24)	16 (24)
Number (%) of Plies in Spar Webs	12 (23)	8 (15)	32 (61)
Number (%) of Plies in Spar Flange	12 (14)	46 (54)	26 (30)
Number (%) of Plies in Panel Stiffeners	38 (61)	4 (6)	20 (32)

6. Conclusions

The present study focuses on weight minimization of laminated wing torsion box structure by alteration of ply orientations and deleting non-contributing plies using GA. The reference outer geometry of wing was taken from DLR-F6 aircraft, while its internal structure was designed based on the basic formulations of aircraft structural design for aircraft's design all up weight requirement. To optimize wing panels, spars, webs and stiffeners a single-objective fitness function was designed as a combination of multi-objective design criterion. The fitness function connects wing tip deflection, first ply failure index (based on Tsai-Wu criterion) and assembly weight design criterion to a single platform with the use of weight factors and scaling factors for optimization. The choice of weight factors in fitness function was based on series of Pareto fronts obtained from the 3D scatter plots of feasible solutions. The GA based optimization algorithm for minimization of fitness function was developed in MATLAB and submitted to ABAQUS/CAE for function evaluations. The GA chromosomes participating in optimization have been defined to have ply orientation and ply-

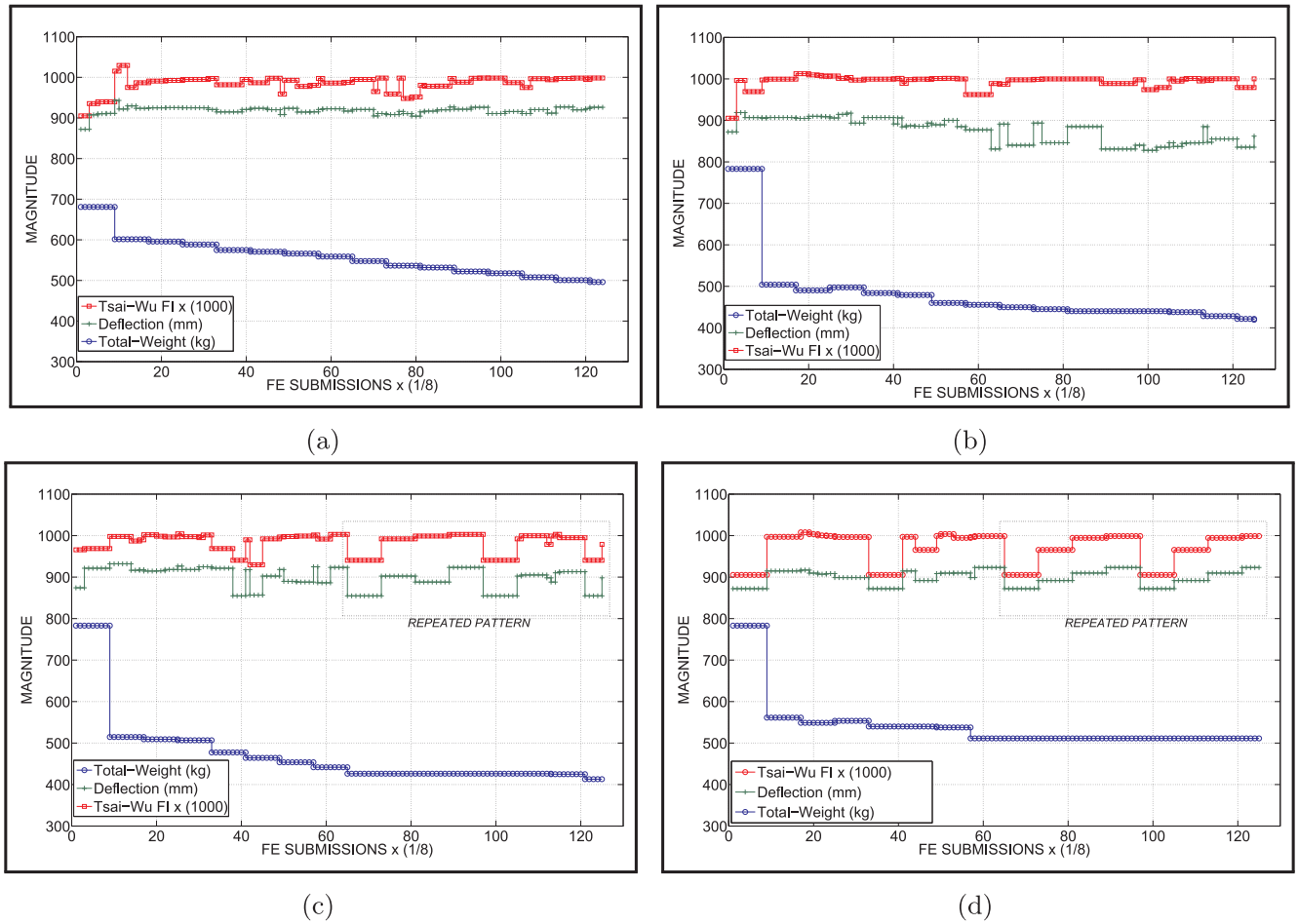

Fig. 17. Effect of mutation percentage (X) on convergence (a) $X = 1\%$ (b) $X = 10\%$ (c) $X = 25\%$ (d) $X = 50\%$.

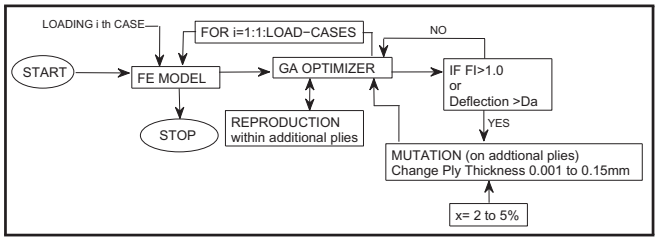

Fig. 18. Submission of other load cases.

existence information within laminate. The individual laminate definition was updated as outcome of the present study.

The following are the key conclusions that can be drawn from the present study.

(a) The fitness function for GA optimization was established to minimize the assembly weight using scaling factors and a weight vector. The scaling factor normalizes the design criterion while the weight vector prioritizes them during optimization. In the present problem, the weight vector priority was in such a manner that assembly weight reduction should be done only when other design parameters are within design allowable limits. However, incorrect selection of weight vector showed that the algorithm can bring down assembly weight but at the cost of violation of design limits. This indicates that the selection of weight vector plays very important role towards the solution convergence.

(b) The 3D plots between design criteria showed that the problem has convex Pareto front under different choices of weight vectors. The Pareto front was found to be emerging from the point on bottom most parallel plane of *D* and *FI* axes. The frontal shape of 3D plot was essentially convex as this problem was about minimization of a single objective, while other two objectives have to be within design allowable limits irrespective of minimization. Therefore, the weight vector selection must be based on a posteriori articulation for such structural design problems.

(c) The LSS decides the sequence of laminate selection during optimization based on maximum value of *FI*. The LSS breaks the sequential flow of the process and guides the solution sequence to the laminate where *FI* criterion is getting violated. The violation of *FI* frequently occurs during optimization as there is large difference in strength and elastic modulus with fiber orientation.

(d) The optimization brought out new laminates of lesser weight which are structurally strong and in compliance with set stiffness criterion. The laminated structure when compared with its metallic counterpart, showed almost 599 kg (that is, about 54%) reduction in weight.

(e) The application of GA which governed FE solutions for multi-objective multi-laminate wing optimization, emerged as a highly effective tool and showed almost 201 kg (29%) of structural weight reduction and 30% less number of plies when compared to an initial quasi-isotropic laminated structure.

(f) The optimal laminate indicates that almost 50–60% ply orientations for panel, stiffener laminates are principally aligned to take care of tensile loads due to wing bending and that of the spar-web laminates are principally aligned to take care of shear loads. Therefore, present analysis suggests that without doing optimization one can use 50% plies in-line with principal load direction for panels, stiffeners and spar-web, while the spar-flange material has 50% plies with 90° orientation from the bending axis.

(g) A careful choice of percentage of mutation is very important in deciding convergence rate of GA optimization process. The low value (1–2%) of mutation leads to local optima. On the other hand, high value (25–50%) of mutation damages the entire good characteristics of the parent strings. Thus the new-string becomes unacceptable in iterative process and solution leads to a pre-matured convergence state. In present study, 10% mutation was found to be a reasonable choice after a series of initial solutions.

(h) The time requirement for FE analyses on a medium range computational facility for present study was found to be minimal with use of structured global mesh. Therefore, with well structured global mesh along with GA, one can do optimization of large multi-laminated aerospace structural problems in a pragmatic time line.

References

[1] Shrivastava S, Mohite P. Design and optimization of a composite canard control surface of an advanced fighter aircraft under static loading. Curved Layered Struct 2015;2(1):91–105. http://dx.doi.org/10.1515/cls-2015-0006.
[2] Deb K. Optimization for engineering design: algorithms and examples. India: Prentice-Hall of India9788120309432; 2004.
[3] Miettinen K, Ruiz F, Wierzbicki A. Introduction to Multiobjective Optimization: Interactive Approaches. In: Branke J, Deb K, Miettinen K, Slowinski R. (Eds.,) Multiobjective Optimization. Lecture Notes in Computer Science. Berlin, Heidelberg: Springer; 2008. ISBN 978-3-540-88907-6.
[4] Almeida F, Awruch A. Design optimization of composite laminated structures using genetic algorithms and finite element analysis. Compos Struct 2009;88(3):443–54. http://dx.doi.org/10.1016/j.compstruct.2008.05.004.
[5] Karakaya S, Soykasap O. Buckling optimization of laminated composite plates using genetic algorithm and generalized pattern search algorithm. Struct Multidiscip Optim 2009;39(5):477–86. http://dx.doi.org/10.1007/s00158-008-0344-2.
[6] Diaconu C, Sekine H. Layup optimization for buckling of laminated composite shells with restricted layer angles. AIAA 2004;42(10):2153–63. http://dx.doi.org/10.2514/1.931.
[7] Ijsselmuiden S, Abdalla M, Gürdal Z. Optimization of variable-stiffness panels for maximum buckling load using lamination parameters. AIAA 2010;48(1):134–43. http://dx.doi.org/10.2514/1.42490.
[8] Deka D, Sandeep G, Chakraborty D, Dutta A. Multiobjective optimization of laminated composites using finite element method and genetic algorithm. Reinf Plast Compos 2005;24(3):273–85. http://dx.doi.org/10.1177/0731684405043555.
[9] Kalantari M, Dong C, Davies I. Multi-objective robust optimisation of unidirectional carbon/glass fibre reinforced hybrid composites under flexural loading. Compos Struct 2016;138:264–75. http://dx.doi.org/10.1016/j.compstruct.2015.11.034.
[10] Lee D, Morillo C, Oller S, Bugeda G, Onate E. Robust design optimisation of advance hybrid (fibermetal) composite structures. Compos Struct 2013;99:181–92. http://dx.doi.org/10.1016/j.compstruct.2012.11.033.
[11] Sasidhar G, Moses D, Mallesam D. Multiobjective optimization of laminated composites plate using a non-dominated sorting genetic algorithm. Eng Sci Technol 2013;5(4):844–9. http://citeseerx.ist.psu.edu/viewdoc/summary?doi=10.1.1.295.423.
[12] Topal U, Uzman Ü. Frequency optimization of laminated composite angle-ply plates with circular hole. Mater Des 2008;29(8):1512–7. http://dx.doi.org/10.1016/j.matdes.2008.03.002.
[13] Kim Y, Jeon Y, Lee D. Multi-objective and multidisciplinary design optimization of supersonic fighter wing. Aircraft 2006;43(3):817–24. http://dx.doi.org/10.2514/1.13864.
[14] Madeira J, Arajo A, Soares CM, Soares CM, Ferreira A. Multiobjective design of viscoelastic laminated composite sandwich panels. Compos Part B 2015;77:391–401. http://dx.doi.org/10.1016/j.compositesb.2015.03.025.
[15] Gillet A, Francescato P, Saffre P. Single and multi-objective optimization of composite structures: the influence of design variables. Compos Mater 2010;44(4):457–80. http://dx.doi.org/10.1177/0021998309344931.
[16] Deb K, Pratap A, Agarwal S, Meyarivan T. A fast and elitist multi-objective genetic algorithm: Nsga-ii. IEEE Trans Evol Comput 2002;6(2):182–97. http://www.sciencedirect.com/science/article/pii/096195269290001M.
[17] Blasques J, Stolpe M. Maximum stiffness and minimum weight optimization of laminated composite beams using continuous fiber angles. Struct Multidisc Optim 2011;43:573–88. http://dx.doi.org/10.1007/s00158-010-0592-9.
[18] Cai H, Aref A. A genetic algorithm-based multi-objective optimization for hybrid fiber reinforced polymeric deck and cable system of cable-stayed bridges. Struct Multidiscip Optim 2015;52(3):583–94. http://dx.doi.org/10.1007/s00158-015-1266-4.
[19] Pelletier J, Vel S. Multi-objective optimization of fiber reinforced composite laminates for strength, stiffness and minimal mass. Comput Struct 2006;84(29–30):2065–80. http://dx.doi.org/10.1016/j.compstruc.2006.06.001.
[20] Hemmatian H, Fereidoon A, Sadollah A, Bahreininejad A. Optimization of laminate stacking sequence for minimizing weight and cost using elitist ant system optimization. Adv Eng Softw 2013;57:8–18. http://dx.doi.org/10.1016/j.advengsoft.2012.11.005.
[21] Mallela U, Upadhyay A. Buckling load prediction of laminated composite stiffened panels subjected to in-plane shear using artificial neural networks. Thin-walled Struct 2016;102:158–64. http://dx.doi.org/10.1016/j.tws.2016.01.025.
[22] Artero-Guerrero J, Pernas-Snchez J, Martin-Montal J, Varas V, Lpez-Puente J. The influence of laminate stacking sequence on ballistic limit using a combined experimental/fem/artificial neural networks (ann) methodology. Compos Struct 2017. http://dx.doi.org/10.1016/j.compstruct.2017.03.068.
[23] Vassberg J, Tinoco E, Mani M, Brodersen O, Eisfeld B, Wahls R, et al. Abridged summary of the third aiaa computational fluid dynamics drag prediction workshop. J Aircraft 2008;45(3):781–98. http://dx.doi.org/10.2514/1.30572.

[24] Wang Z. Adaptive high-order methods in computational fluid dynamics. Advances in computational fluid dynamics. Singapore: World Scientific9789814313186; 2011.
[25] ANSYS FLUENT Theory Guide, Release 14.5. ANSYS; 2014.
[26] Gunter E, McDonnnell D. DC-9/MD-80 and MD-90. London: Ian Allan0711019584; 1991.
[27] Howe D. Aircraft conceptual design synthesis. aerospace series. United Kingdom: Professional Engineering Publishing9781860583018; 2000.
[28] Gudmundsson S. General Aviation Aircraft Design: Applied Methods and Procedures. Brazil: Elsevier Science9780123973290; 2013.
[29] Kaw A. Mechanics of Composite Materials. Mechanical and Aerospace Engineering Series. United Kingdom: Taylor & Francis9780849396564; 1997.
[30] Herakovich C. Mechanics of Fibrous Composites. New Jersey, US: John Wiley9780471106364; 1997.
[31] Koerber H, Camanho P. High strain rate characterisation of unidirectional carbonepoxy im7-8552 in longitudinal compression. Compos Part A Appl Sci Manuf 2011;42(5):462–70. http://dx.doi.org/10.1016/j.compositesa.2011.01.002.
[32] ABAQUS/Standard User's Manual, Version 6.11. Simulia; 2011.
[33] Srinivas N, Deb K. Multiobjective optimization using nondominated sorting in genetic algorithms. Evol Comput 1994;2(3):221–48. http://dx.doi.org/10.1162/evco.1994.2.3.221.
[34] Ball N, Sargent P, Ige D. Genetic algorithm representations for laminate layups. Artif Intell Eng 1993;8(2):99–108. http://dx.doi.org/10.1016/0954-1810(93)90020-G.
[35] Jubril A. A nonlinear weight selection in weighted sum for convex multi-objective optimization. Ser Math Inform 2012;27(3):357–72.
[36] Haupt R, Haupt S. Practical genetic algorithms. New York, USA: John Wiley and Sons, Inc.047-1188735; 1998.
[37] Tsai S, Wu E. A general theory of strength for anisotropic materials. Compos Mater 1971;5(1):58–80. http://dx.doi.org/10.1177/002199837100500106.
[38] Miettinen K. A Posteriori Methods. Boston, MA: Springer978-1-4613-7544-9; 1998. http://dx.doi.org/10.1007/978-1-4615-5563-6.